Highly Efficient Spin-to-Charge Current Conversion in Strained HgTe Surface States Protected by a HgCdTe Layer

P. Noel,[1] C. Thomas,[2] Y. Fu,[1] L. Vila,[1] B. Haas,[3] P-H. Jouneau,[3] S. Gambarelli,[4] T. Meunier,[5] P. Ballet,[2] and J. P. Attané[1,*]
[1]*Univ. Grenoble Alpes, CEA, CNRS, Grenoble INP, INAC, SPINTEC, F-38000 Grenoble, France*
[2]*Univ. Grenoble Alpes, CEA, LETI, MINATEC Campus, F38054 Grenoble, France*
[3]*CEA, INAC-MEM, 38054 Grenoble, France*
[4]*CEA, Institut Nanosciences et Cryogénie, SyMMES F-38000 Grenoble, France*
[5]*CNRS, Institut NEEL, 38042 Grenoble, France*

(Received 21 July 2017; revised manuscript received 8 March 2018; published 16 April 2018)

We report the observation of spin-to-charge current conversion in strained mercury telluride at room temperature, using spin pumping experiments. We show that a HgCdTe barrier can be used to protect the HgTe from direct contact with the ferromagnet, leading to very high conversion rates, with inverse Edelstein lengths up to 2.0 ± 0.5 nm. The influence of the HgTe layer thickness on the conversion efficiency is found to differ strongly from what is expected in spin Hall effect systems. These measurements, associated with the temperature dependence of the resistivity, suggest that these high conversion rates are due to the spin momentum locking property of HgTe surface states.

DOI: 10.1103/PhysRevLett.120.167201

Conventional spintronics is based upon the use of magnetic materials to manipulate spin currents [1]. Such a manipulation can be achieved by harnessing the spin-orbit coupling in nonmagnetic materials. For instance, the spin Hall effect [2] permits one to convert charge currents into spin currents in the bulk of heavy metals. It has also been recently demonstrated that higher conversion rates can be obtained by using two-dimensional electron gas with high spin-orbit coupling, in Rashba interfaces [3] or at topological insulator (TIs) surfaces [4–7]. As a consequence, the use of Rashba interfaces, such as Ag/Bi [8,9] or SrTiO3/LaAlO3 [10], and of various TIs [11–15] is generating a growing attention in spintronics.

The main interest of TIs lies in their surface states, which possess a linear Dirac-like energy dispersion, and in the perpendicular locking between spin and momentum [4–7]. A flow of electric current in the two-dimensional electron gas gives rise to a perpendicular spin accumulation, this effect being known as the Edelstein effect [16], while the reverse spin-to-charge conversion phenomenon is known as the inverse Edelstein effect (IEE) [17].

The conversion has been observed in various Bi-based TIs such as Bi_2Se_3 [11,12], BiSbTeSe [14] or Sn-doped BiTeSe [15]. Although large spin torque efficiencies have been measured in Bi_2Se_3 [18], this system exhibits at room temperature relatively low surface related spin-to-charge conversion rates [19]. Because of intrinsic doping by selenium vacancies, Bi_2Se_3 presents bulk metallic states. In bulk-insulating BiSbTeSe and Sn-doped BiTeSe, a high conversion rate has been observed by spin pumping, but only at low temperature. The conversion has also been observed in strained α-Sn [13], but in order to preserve the Dirac cone, a conductive layer has to be inserted between the ferromagnetic layer and the surface states, inducing a large magnetic damping, which could limit its interest for spin-orbit torques.

In that context, strained HgTe is a TI expected to exhibit high conversion rates, as is characterized by a very high mobility of its surface states [20]. Moreover, HgTe/CdTe is an archetypal topological insulator [21], compatible with electronic [22,23] and commercial optoelectronic applications [24]. Beyond classical spintronic applications, such as current-induced magnetization switching, its compatibility with optronics devices can pave the way toward new devices combining spintronics and photonics in the IR and terahertz range [25–27].

In this Letter, we demonstrate the spin-to-charge current conversion at room temperature in strained HgTe. Using spin pumping, we measure a very high conversion efficiency. We show that a HgCdTe barrier can be used to protect the HgTe surface states from direct contact with the ferromagnet, leading to an enhancement of the conversion rate. We then show that the dependence of the conversion with the HgTe thickness differs from the usual dependence observed in spin Hall materials. In particular, the maximal conversion efficiency is obtained in a regime for which the top and bottom surface states are still hybridized. These dependences, associated with the temperature dependence of the resistivity, suggest that the high conversion rate can be attributed to the spin momentum locking at the surface states of HgTe.

Strained HgTe is known to be a TI with Dirac surface states [20,21,28]. The light hole band $\Gamma_{8,LH}$ is lying 0.3 eV above the Γ_6 band. Such an inverted band structure at the Γ

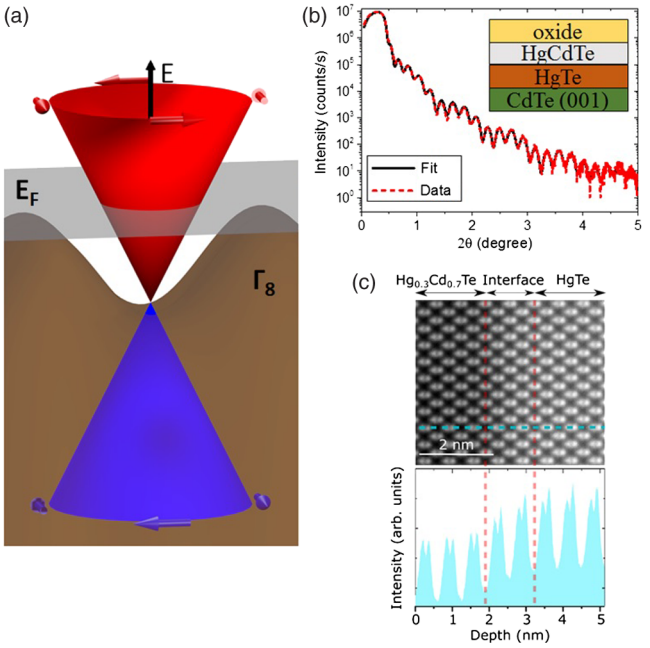

FIG. 1. (a) Schematic representation of the band structure of strained HgTe, with the Dirac dispersion cone of the surface states, and the bulk Γ_8 band. The arrows represent the helical spin configuration. (b) X-ray reflectivity spectrum of a HgTe (18.5 nm)/HgCdTe (5.5 nm) sample. The structure used for the fit is represented in the inset. The red dashed curve represents the experimental data; the black curve is the fit. (c) Scanning tunneling electron microscopy HAADF image of HgCdTe/HgTe/HgCdTe structure and corresponding chemical profile.

point results in topological surface states, robust to the presence of the heavy hole band $\Gamma_{8,\mathrm{HH}}$ [cf. Fig. 1(a)]. Band gap opening and TI properties can then be induced in HgTe by applying a tensile strain, which lifts the degeneracy at the Γ point. Experimentally, the tensile strain state can be achieved by growing HgTe on a substrate having a larger lattice constant, such as CdTe. In these conditions, the existence of a Dirac cone at the free surface of HgTe has been confirmed by angle resolved photoemission spectroscopy (ARPES) measurements [29].

Here, HgTe thin films have been grown by molecular beam epitaxy (the growth conditions are detailed in Refs. [30,31]). After the deposition on a CdTe (001) substrate of a 200 nm thick CdTe buffer layer, a strained HgTe layer (10–80 nm thick) has been grown, immediately capped with a 5 nm thick $Hg_{0,3}Cd_{0,7}Te$ layer to avoid any Hg desorption. After deposition, the thicknesses of both the HgTe and HgCdTe layers have been measured by x-ray reflectivity (XRR) as seen in Fig. 1(b)[32]. The estimated roughness for the HgTe layer and HgCdTe capping was inferior to 0.5 nm. The crystallographic quality of the heterostructure and the sharpness of the HgTe/HgCdTe interface have also been controlled by high-angle annular dark-field (HAADF) imaging in a scanning transmission electron microscope [cf. Fig. 1(c)] [33]. The associated intensity profile allows for the marking of the interface chemical boundaries between HgTe and $Hg_{0.7}Cd_{0.3}Te$. The interface width of 1.4 nm has to be considered as an upper bound as the intensity profile is averaged over the 50–100 nm thickness of the focused-ion-beam-prepared lamellae.

To perform spin pumping experiments, a 20 nm thick NiFe layer has been deposited *ex situ* by evaporation. A soft Ar etching has been performed prior to the NiFe deposition, in order to remove the oxide layer and eventually to modulate the thickness of the HgCdTe barrier.

After the deposition of the NiFe layer, the thicknesses of the NiFe and HgCdTe films have been measured by XRR. The samples have then been cut into 0.4 mm wide and 2.4 mm long stripes, before being measured by conventional spin pumping ferromagnetic resonance experiments in cavity [34]. A static magnetic field H has been applied in the plane of the sample, while a radio frequency field h_{rf} at 9.68 GHz has been applied perpendicularly, thus leading the magnetization of the NiFe thin film to precess [cf. Fig. 2(a)].

At the ferromagnetic resonance, a pure spin current flows from the NiFe/HgCdTe interface toward the HgTe layer [35]. This flow is evidenced by the increase of the Gilbert damping α, revealing the extra magnetic relaxation channel that appears when adding the HgCdTe/HgTe/CdTe stack

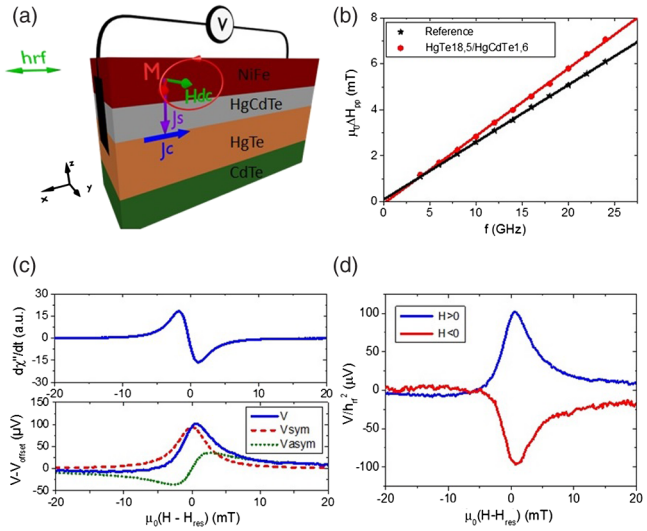

FIG. 2. (a) Principle of the spin pumping FMR measurement. (b) Broadband frequency dependence of the peak-to-peak FMR linewidth of the reference NiFe/Si sample and of a NiFe/HgCdTe(1.6)/HgTe(18.5) sample. The damping coefficient of NiFe is higher when deposited on HgTe ($\alpha_{\mathrm{ref}} = 6.33 \times 10^{-3} \pm 3 \times 10^{-5}$ for the reference sample compared to $\alpha = 7.50 \times 10^{-3} \pm 7 \times 10^{-5}$). For a rf field of 0.1 mT, this leads to a pure spin current $J_s^{3D} = 7.6 \pm 0.2$ MA/m^2. (c) FMR and dc voltages, measured by spin pumping FMR on the same sample. The symmetric (red) and antisymmetric (green) contributions have been extracted from the measured signal (in blue). (d) Spin pumping signals obtained for a positive and a negative dc field, on the same sample.

to the NiFe layer. The damping parameter α can be extracted from the linear dependence of the peak-to-peak linewidth ΔH_{pp} with the frequency f of the rf field using stripline broadband ferromagnetic resonance (FMR) [cf. Fig. 2(b)]

$$\Delta H_{\mathrm{pp}} = \Delta H_0 + \frac{2}{\sqrt{3}}\left(\frac{2f}{\gamma}\right)\alpha,$$

where γ is the gyromagnetic ratio and ΔH_0 is the inhomogeneous contribution to the linewidth.

The extra Gilbert damping $\Delta\alpha$ due to the spin pumping is calculated by comparing the damping parameter of a reference NiFe(20nm)//Si sample ($\alpha = 6.33 \pm 0.03 \times 10^{-3}$) to those of the NiFe/HgCdTe/HgTe//CdTe samples. This extra damping is in the range of 0.1×10^{-3} to 2×10^{-3} for all studied samples, more than 10 times smaller than the damping induced by Pt or α-Sn [13]. Such low values underline the potential of HgTe for spin torque experiments, as the switching current, dominated by the αM_s^2 term [36], could be significantly reduced in this system.

The extraction of the conversion efficiency has been done using the model proposed by Mosendz *et al.* [37]. The extra damping $\Delta\alpha$ is related to the effective spin mixing conductivity $G_{\mathrm{eff}}^{\uparrow\downarrow}$, which expresses the global spin transmission

$$G_{\mathrm{eff}}^{\uparrow\downarrow} = \frac{4\pi M_s t_{\mathrm{NiFe}}}{g\mu_B}\Delta\alpha,$$

where t_{NiFe} is the thickness of the NiFe layer (20 nm), g is the Landé factor of NiFe, $\mu_0 M_s$ is the saturation magnetization, and μ_B is the Bohr magneton. At the ferromagnetic resonance, a spin current appears, directed vertically from the NiFe layer toward the strained HgTe. Its density J_s^{3D} can be written [35] as

$$J_s^{\mathrm{3D}} = \frac{G_{\mathrm{eff}}^{\uparrow\downarrow}\gamma^2\hbar h_{\mathrm{rf}}^2}{8\pi\alpha^2}\left(\frac{4\pi M_s\gamma + \sqrt{(4\pi M_s\gamma)^2 + 4\omega^2}}{(4\pi M_s\gamma)^2 + 4\omega^2}\right)\frac{2e}{\hbar},$$

where ω is the angular frequency of the rf field. This pure spin current can then be converted into a transverse dc charge current I_C, by inverse spin Hall effect (ISHE) or IEE [34,35,37].

Figure 2(c) presents the ferromagnetic resonance signal, together with the spin pumping signal, for an 18.5 nm thick HgTe sample covered by a 1.6 nm thick HgCdTe layer. As can be seen in Figs. 2(c) and 2(d), the signal is mostly symmetrical with respect to the resonance field, and its sign is well reversed when turning the sample by 180°, which implies that $V(H)$ is dominated by the IEE or ISHE contributions and that the anomalous Hall and Seebeck effects are negligible (see Supplemental Material [38]).

The most striking result is the presence of a very efficient conversion at room temperature: the produced charge current density $J_c = I_c/w$, with w, the width of the sample, is found to be much larger (up to 4.25 mA/m) than what can be obtained with heavy metals (e.g., 1.25 mA/m in a thick Pt sample [42,43]) and on the same order of magnitude as the highest value reported to our knowledge (5 mA/m in alpha-Sn [13]).

Let us now focus on the role of the HgCdTe barrier. The direct contact from a metal with a TI is known to be detrimental to the conversion efficiency, because of the decrease of the carrier lifetime [13,44], of Fermi level variation [45,46], or of the modification of the interface chemistry [47]. Thus, several theoretical studies underlined the necessity to protect the surface states with an insulating layer [44,45], but without experimental demonstration yet.

Here we study the dependence of the charge current with the HgCdTe barrier thickness [cf. Figs. 3(a) and 3(b)]. As expected theoretically, thin HgCdTe barriers, from 0.6 to 3 nm, allow one to obtain higher currents than the direct contact between NiFe and HgTe. Nonetheless, as the barrier thickness is increased, the signal decreases. A control sample with a 17 nm thick HgCdTe barrier has been deposited, showing a signal 2 orders of magnitude smaller ($J_c/J_{c\,\max} = 3\%$) [48]. This extinction confirms that the observed conversion does not occur at the NiFe/HgCdTe interface. The decrease of the signal with the barrier points toward a decrease of the electronic coupling through the

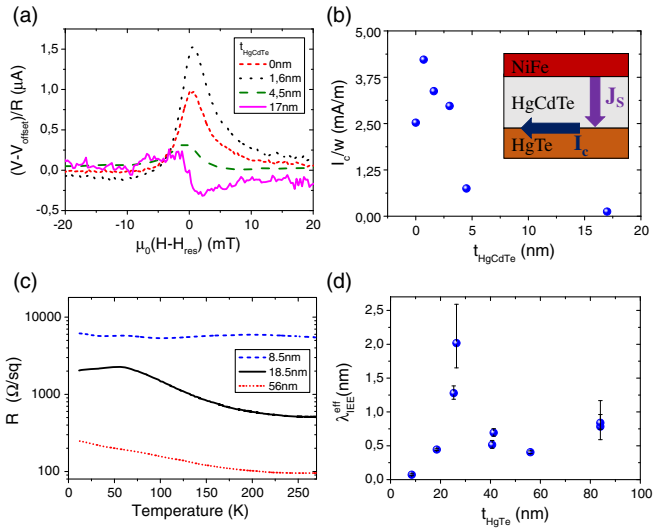

FIG. 3. (a) Spin pumping signals obtained for different thicknesses of HgCdTe barriers, normalized by the sample resistance. (b) HgCdTe thickness dependence of I_C/w. The measurements were all performed on HgTe layers of the same thickness (18.5 nm), while varying the HgCdTe layer thickness using Ar etching. The thicknesses were measured by XRR. (Inset) Scheme of the conversion. (c) Sheet resistance R_{sheet} as a function of the temperature, for three samples of different HgTe thicknesses (8.5, 18.5, and 56 nm). (d) HgTe thickness dependence of the inverse Edelstein length λ_{IEE}. The HgCdTe barrier thickness is the same for all the samples ($t_{\mathrm{HgCdTe}} \sim 1.6$ nm). The large error bars for the 26 and 84 nm thick samples are due to a relatively large uncertainty on the extra damping.

insulating HgCdTe. As in a Si barrier [49], apart from quantum tunneling, residual doping and carriers in the HgCdTe barrier could lead to indirect exchange process or spin diffusion mechanisms.

Note that measurements with a Cu spacer layer instead of HgCdTe have also been performed. They exhibit a larger damping parameter and considerably smaller conversion efficiencies, even in comparison with NiFe in direct contact [38]. This suggests that the conversion efficiency is highly dependent on the metal in contact and that careful attention to the choice of the interlayer is needed.

An important question remains regarding the respective role of bulk and surface states. The temperature dependence of the sheet resistance has been studied for different HgTe thicknesses [see Fig. 3(c)]. A resistance maximum is observed at around 50 K for the 18.5 nm thick HgTe layer. Its existence suggests the presence of two parallel channels of conduction, the first one corresponding to the bulk of HgTe, with a resistivity decrease when increasing the temperature, the second one corresponding to the topological surface states, dominating the conductivity at low temperature. When increasing the HgTe thickness to 56 nm, the bulk contribution dominates the signal: the resistance keeps increasing at low temperature, without any signature of metallic behavior. For a thinner (8.5 nm) sample, where the bulk contribution is expected to be reduced, there is no overall increase of the sheet resistance when decreasing temperature. The presence of both bulk and surface state conduction can also be seen in Hall measurements [38]. At 300 K, the transport is dominated by an n-type contribution due to thermally activated bulk charge carriers, whereas at 10 K, both bulk p- and n-type surface state contributions are observed.

Let us now estimate the spin-to-charge conversion factor, i.e., the ratio of the obtained to the injected current densities. This value, which denotes the efficiency of the conversion from a spin current J_s^{3D} (in A/m^2) into a surface charge current J_c^{2D} (in A/m), is known as the inverse Edelstein length λ_{IEE},

$$\lambda_{IEE} = \frac{J_c^{2D}}{J_s^{3D}} = \frac{I_C}{wJ_s^{3D}}.$$

Figure 3(d) shows the dependence of λ_{IEE}, with the HgTe thickness at a fixed HgCdTe thickness of 1.6 nm. If the dependence was due to the spin Hall effect (SHE) in HgTe, we would expect a hyperbolic tangent increase with the HgTe thickness, i.e., $(I_c/J_s^{3D}) \propto \tanh(t/2l_{sf})$, with t being the HgTe thickness and l_{sf} its spin diffusion length [35]. The observed dependence is very different, with a large increase of λ_{IEE} from $t = 8.5$ to 26 nm, where the highest Inverse Edelstein length is obtained, and after which the efficiency drops.

In an ideal topological insulator, the inverse Edelstein length is equal to the product of the mean free path of the surface states λ by the spin polarization of the surface states P [44]. Yet if the bulk is not perfectly insulating, it acts as an additional relaxation channel [14], as scattering on the bulk states can occur, and the inverse Edelstein length is reduced. Using the empirical model of Ref. [15] leads to $\lambda_{IEE} = P\lambda R_b/(R_b + R_s)$, where R_b and R_s are the sheet resistance for the bulk and surface states, respectively. The existence of a large bulk contribution explains the decrease of λ_{IEE} for thick HgTe layers observed in Fig. 3(d).

λ_{IEE} also decreases at HgTe thicknesses below 26 nm. A possible origin of this decrease is the hybridization of the upper and lower HgTe surfaces. Because of the overlap of the two wave functions, an electronic transport through states delocalized between the surfaces can be observed [50], where the spin degeneracy is restored. As a consequence, the spin momentum locking properties, and thus the polarization and the spin-to-charge conversion efficiency, are expected to progressively disappear as the thickness of the TI shrinks [51]. Interestingly, the maximal conversion efficiency is obtained when the top and bottom surface states are still hybridized. This result is in agreement with theoretical predictions for systems in which the bulk contribution to the relaxation cannot be neglected [52]. Although the analogy with Bi-based TIs has to be taken cautiously, recent measurements on Bi_2Se_3 also suggest that the conversion efficiency is maximal when surface states are still hybridized and reduced at larger thicknesses [53].

The thickness below which the decrease is observed is 26 nm. This value is consistent with the hypothesis that the main origin of the decrease is the hybridization, as the wave function extension is predicted to be on the order of 5 nm [33,54]. Additionally, for the thinnest sample (8.5 nm), the low conversion rate could be due to the lack of band inversion at room temperature [55] and to the absence of surface states.

Note that the conversion remains large at low temperature. HgTe samples of 26.4 and 56 nm thicknesses have been measured at 15 K, when the bulk states are expected to be frozen, without modifying strongly the current production [38]. Note also that the thickness dependence of the electronic properties in HgTe is complex [28,55–57], and that further experiments and theoretical works are required for a better understanding of the conversion rate evolution with the HgTe thickness.

Another interesting feature of the spin pumping method is its ability to determine the chirality of the Fermi circle. According to Hall and ARPES measurements [29,50], in ungated samples, the Fermi level is expected to be above the Dirac point. Because λ_{IEE} is positive, this indicates that the helical Fermi contour is counterclockwise in the upper part of the cone [as illustrated in Fig. 1(a)], in accordance with predictions [58].

Beyond its sign, the amplitude of the conversion rate is noteworthy. The conversion rate λ_{IEE} can reach a value of 2.0 ± 0.5 nm, comparable to that of alpha-Sn ($\lambda_{IEE} = 2.1$ nm in Ref. [13]), i.e., the highest value recorded up to now at room temperature. Note that λ_{IEE}

can also be compared to the product of the SHE angle by the spin diffusion length $\theta_{\mathrm{SHE}} l_{sf}$ [9]. In the case of SHE materials such as Pt, the reported value is 0.57 nm [59]. This value is one or two of magnitude larger than the obtained value in Bi-based systems [14,15,19] and can be ascribed to the higher value of the mobility and mean free path in HgTe [15,20,60].

To conclude, we observed at room temperature the spin-to-charge current conversion in the topological surface states of strained HgTe, with a counterclockwise direction of the spin rotation and very high conversion rates. As expected theoretically, the conversion can be optimized using a HgCdTe barrier. To obtain the highest conversion rate, it seems that the HgTe layer thickness has to be thick enough to decouple the top and bottom surface, but thin enough to avoid the relaxation within the bulk.

These results underline the necessity to add an interlayer between the TI and ferromagnetic metal to obtain high conversion efficiencies, and show that insulating layers are good candidates to protect the TI surface states. The HgTe thickness dependence of the conversion rate is strongly different from SHE materials, suggesting that several mechanisms, such as hybridization, might play a key role. The gate dependence of the effect remains to be studied, and one can expect to enhance, or at least modulate, the conversion rate [10]. This degree of freedom, and the compatibility of the CdTe/HgTe system IR optronics, make it a very good candidate for applications mixing conventional optronics, spin-optronics phenomena in TIs [25–27], and nonvolatile applications such as three-terminal magnetic random-access memory or magnetoelectric spin orbit logic [61].

We acknowledge the financial support by ANR French National Research Agency Toprise (ANR-16-CE24-0017) and Laboratoire d'excellence LANEF (ANR-10-LABX-51-01). We thank J.-F. Jacquot for the preparation of the samples.

*Corresponding author.
jean-philippe.attane@cea.fr

[1] I. Zutíc, J. Fabian, and S. D. Sarma, Rev. Mod. Phys. **76**, 323 (2004).
[2] J. E. Hirsch, Phys. Rev. Lett. **83**, 1834 (1999).
[3] C. R. Ast, J. Henk, A. Ernst, L. Moreschini, M. C. Falub, D. Pacilé, P. Bruno, K. Kern, and M. Grioni, Phys. Rev. Lett. **98**, 186807 (2007).
[4] Liang Fu, C. L. Kane, and E. J. Mele, Phys. Rev. Lett. **98**, 106803 (2007).
[5] H. Zhang, C. X. Liu, X. L. Qi, X. Dai, Z. Fang, and S. C. Zhang, Nat. Phys. **5**, 438 (2009).
[6] Y. L. Chen, J. G. Analytis, J.-H. Chu, Z. K. Liu, S.-K. Mo, X. L. Qi, H. J. Zhang, D. H. Lu, X. Dai, Z. Fang, S. C. Zhang, I. R. Fisher, Z. Hussain, and Z.-X. Shen, Science **325**, 178 (2009).
[7] M. Z. Hasan and C. L. Kane, Rev. Mod. Phys. **82**, 3045 (2010).
[8] H. J. Zhang, S. Yamamoto, B. Gu, H. Li, M. Maekawa, Y. Fukaya, and A. Kawasuso, Phys. Rev. Lett. **114**, 166602 (2015).
[9] J.-C. Rojas-Sánchez, L. Vila, G. Desfonds, S. Gambarelli, J. P. Attané, J. M. De Teresa, C. Magén, and A. Fert, Nat. Commun. **4**, 2944 (2013).
[10] E. Lesne, Y. Fu, S. Oyarzun, J. C. Rojas-Sánchez, D. C. Vaz, H. Naganuma, G. Sicoli, J.-P. Attané, M. Jamet, E. Jacquet, J.-M. George, A. Barthélémy, H. Jaffrès, A. Fert, M. Bibes,, and L. Vila, Nat. Mater. **15**, 1261 (2016).
[11] A. R. Mellnik, J. S. Lee, A. Richardella, J. L. Grab, P. J. Mintun, M. H. Fischer, A. Vaezi, A. Manchon, E.-A. Kim, N. Samarth, and D. C. Ralph, Nature (London) **511**, 449 (2014).
[12] M. Jamali, J. S. Lee, J. S. Jeong, F. Mahfouzi, Y. Lv, Z. Zhao, B. K. Nikolić, K. A. Mkhoyan, N. Samarth, and J.-P. Wang, Nano Lett. **15**, 7126 (2015).
[13] J.-C. Rojas-Sánchez, S. Oyarzún, Y. Fu, A. Marty, C. Vergnaud, S. Gambarelli, L. Vila, M. Jamet, Y. Ohtsubo, A. Taleb-Ibrahimi, P. Le Fèvre, F. Bertran, N. Reyren, J.-M. George, and A. Fert, Phys. Rev. Lett. **116**, 096602 (2016).
[14] Y. Shiomi, K. Nomura, Y. Kajiwara, K. Eto, M. Novak, K. Segawa, Y. Ando, and E. Saitoh, Phys. Rev. Lett. **113**, 196601 (2014).
[15] K. T. Yamamoto, Y. Shiomi, K. Segawa, Y. Ando, and E. Saitoh, Phys. Rev. B **94**, 024404 (2016).
[16] V. M. Edelstein, Solid State Commun. **73**, 233 (1990).
[17] K. Shen, G. Vignale, and R. Raimondi, Phys. Rev. Lett. **112**, 096601 (2014).
[18] Y. Wang, P. Deorani, K. Banerjee, N. Koirala, M. Brahlek, S. Oh, and H. Yang, Phys. Rev. Lett. **114**, 257202 (2015).
[19] H. Wang, J. Kally, J. S. Lee, T. Liu, H. Chang, D. R. Hickey, K. A. Mkhoyan, M. Wu, A. Richardella, and N. Samarth, Phys. Rev. Lett. **117**, 076601 (2016).
[20] D. A. Kozlov, Z. D. Kvon, E. B. Olshanetsky, N. N. Mikhailov, S. A. Dvoretsky, and D. Weiss, Phys. Rev. Lett. **112**, 196801 (2014).
[21] L. Fu and C. L. Kane, Phys. Rev. B **76**, 045302 (2007).
[22] D. L. Smith, T. C. McGill, T. J. Watson, and J. N. Schulman, Appl. Phys. Lett. **43**, 180 (1983).
[23] Y. D. Zhou, C. R. Becker, Y. Selamet, Y. Chang, R. Ashokan, R. T. Boreiko, T. AokiDavid, J. Smith, A. L. Betz, and S. Sivananthan, J. Electron. Mater. **32**, 608 (2003).
[24] A. Rogalski, Rep. Prog. Phys. **68**, 2267 (2005).
[25] A. Shuvaev, A. Pimenov, G. V. Astakhov, M. Mühlbauer, C. Brüne, H. Buhmann, and L. W. Molenkamp, Appl. Phys. Lett. **102**, 241902 (2013).
[26] J. W. McIver, D. Hsieh, H. Steinberg, P. Jarillo-Herrero, and N. Gedik, Nat. Nanotechnol. **7**, 96 (2012).
[27] A. Soumyanarayanan, N. Reyren, A. Fert, and C. Panagopoulos, Nature (London) **539**, 509 (2016).
[28] C. Brüne, C. X. Liu, E. G. Novik, E. M. Hankiewicz, H. Buhmann, Y. L. Chen, X. L. Qi, Z. X. Shen, S. C. Zhang, and L. W. Molenkamp, Phys. Rev. Lett. **106**, 126803 (2011).
[29] O. Crauste, Y. Ohtsubo, P. Ballet, P. Delplace, D. Carpentier, C. Bouvier, T. Meunier, A. Taleb-Ibrahimi, and L. P. Levy, arXiv:1307.2008v1.
[30] P. Ballet, C. Thomas, X. Baudry, C. Bouvier, O. Crauste, T. Meunier, G. Badano, M. Veillerot, J. P. Barnes, P. H. Jouneau, and L. P. Levy, J. Electron. Mater. **43**, 2955 (2014).

[31] C. Thomas, X. Baudry, J. P. Barnes, M. Veillerot, P. H. Jouneau, S. Pouget, O. Crauste, T. Meunier, L. P. Lévy, and P. Ballet, J. Cryst. Growth **425**, 195 (2015).

[32] We use the cobalt $K\alpha 1$ wavelength of 1.789 Å. The data are fitted using the `Gen-X` software. As the XRR is performed *ex situ*, the HgCdTe insulating barrier is partially oxidized, and the presence of this oxide is taken into account.

[33] B. Haas, C. Thomas, P-H Jouneau, N. Bernier, T. Meunier, P. Ballet, and J-L Rouvière, Appl. Phys. Lett. **110**, 263102 (2017).

[34] K. Ando, S. Takahashi, J. Ieda, Y. Kajiwara, H. Nakayama, T. Yoshino, K. Harii, Y. Fujikawa, M. Matsuo, S. Maekawa, and E. Saitoh, J. Appl. Phys. **109**, 103913 (2011).

[35] Y. Tserkovnyak, A. Brataas, and G. E. W. Bauer, Phys. Rev. B **66**, 224403 (2002).

[36] L. Liu, C. Pai, Y. Li, H. W. Tseng, D. C. Ralph, and R. A. Buhrman, Science **336**, 555 (2012).

[37] O. Mosendz, V. Vlaminck, J. E. Pearson, F. Y. Fradin, G. E. W. Bauer, S. D. Bader, and A. Hoffmann, Phys. Rev. B **82**, 214403 (2010).

[38] See Supplemental Material at http://link.aps.org/supplemental/10.1103/PhysRevLett.120.167201 for the different contributions to the spin signal, measurements with metal in direct contact with HgTe, spin pumping at low temperature, and magnetotransport measurements, which includes Refs. [39–41].

[39] M. Harder, Y. Gui, and C. M. Hu, Phys. Rep. **661**, 1 (2016).

[40] G. D. Davis, J. Vac. Sci. Technol. A **6**, 1939 (1988).

[41] S. Wiedmann, A. Jost, C. Thienel, C. Brüne, P. Leubner, H. Buhmann, L. W. Molenkamp, J. C. Maan, and U. Zeitler, Phys. Rev. B **91**, 205311 (2015).

[42] H. Nakayama, K. Ando, K. Harii, T. Yoshino, R. Takahashi, Y. Kajiwara, K. Uchida, Y. Fujikawa, and E. Saitoh, Phys. Rev. B **85**, 144408 (2012).

[43] J.-C. Rojas-Sánchez, N. Reyren, P. Laczkowski, W. Savero, J.-P. Attané, C. Deranlot, M. Jamet, J.-M. George, L. Vila, and H. Jaffrès, Phys. Rev. Lett. **112**, 106602 (2014).

[44] S. Zhang and A. Fert, Phys. Rev. B **94**, 184423 (2016).

[45] C. D. Spataru and F. Léonard, Phys. Rev. B **90**, 085115 (2014).

[46] J. Zhang, J. P. Velev, X. Dang, and E. Y. Tsymbal, Phys. Rev. B **94**, 014435 (2016).

[47] L. A. Walsh, C. M. Smyth, A. T. Barton, Q. Wang, Z. Che, R. Yue, J. Kim, M. J. Kim, R. M. Wallace, and C. L. Hinkle, J. Phys. Chem. C **121**, 23551 (2017).

[48] O. Mosendz, J. E. Pearson, F. Y. Fradin, S. D. Bader, and A. Hoffmann, Appl. Phys. Lett. **96**, 022502 (2010).

[49] C. H. Du, H. L. Wang, Y. Pu, T. L. Meyer, P. M. Woodward, F. Y. Yang, and P. C. Hammel, Phys. Rev. Lett. **111**, 247202 (2013).

[50] C. Thomas, O. Crauste, B. Haas, P. H. Jouneau, C. Bäuerle, L. P. Lévy, E. Orignac, D. Carpentier, P. Ballet, and T. Meunier, Phys. Rev. B **96**, 245420 (2017).

[51] M. Neupane, A. Richardella, J. Sánchez-Barriga, S. Xu, N. Alidoust, I. Belopolski, C. Liu, G. Bian, D. Zhang, D. Marchenko, A. Varykhalov, O. Rader, M. Leandersson, T. Balasubramanian, T.-R. Chang, H-T. Jeng, S. Basak, H. Lin, A. Bansil, N. Samarth, and M. Z. Hasan, Nat. Commun. **5**, 3841 (2014).

[52] C. S. Ho, Y. Wang, Z. B. Siu, S. G. Tan, M. B. A. Jalil, and H. Yang, Sci. Rep. **7**, 792 (2017).

[53] Y. Wang, D. Zhu, Y. Wu, Y. Yang, J. Yu, R. Ramaswamy, R. Mishra, S. Shi, M. Elyasi, K-L. Teo, Y. Wu, and H. Yang, Nat. Commun. **8**, 1364 (2017).

[54] K.-M. Dantscher, D. A. Kozlov, P. Olbrich, C. Zoth, P. Faltermeier, M. Lindner, G. V. Budkin, S. A. Tarasenko, V. V. Bel'kov, Z. D. Kvon, N. N. Mikhailov, S. A. Dvoretsky, D. Weiss, B. Jenichen, and S. D. Ganichev, Phys. Rev. B **92**, 165314 (2015).

[55] S. S. Krishtopenko, I. Yahniuk, D. B. But, V. I. Gavrilenko, W. Knap, and F. Teppe, Phys. Rev. B **94**, 245402 (2016).

[56] B. Büttner, C. X. Liu, G. Tkachov, E. G. Novik, C. Brüne, H. Buhmann, E. M. Hankiewicz, P. Recher, B. Trauzettel, S. C. Zhang, and L. W. Molenkamp, Nat. Phys. **7**, 418 (2011).

[57] A. A. Dobretsova, L. S. Braginskii, M. V. Entin, Z. D. Kvon, N. N. Mikhailov, and S. A. Dvoretsky, JETP Lett. **101**, 330 (2015).

[58] F. Kirtschig, J. van den Brink, and C. Ortix, Phys. Rev. B **94**, 235437 (2016).

[59] V. T. Pham, L. Vila, G. Zahnd, A. Marty, W. Savero-Torres, M. Jamet, and J-P. Attané, Nano Lett. **16**, 6755 (2016).

[60] D.-X. Qu, Y. S. Hor, J. Xiong, R. J. Cava, and N. P. Ong, Science **329**, 821 (2010).

[61] S. Manipatruni, D. E. Nikonov, R. Ramesh, H. Li, and I. A. Young, arXiv:1512.05428.